Nonadiabatic Quantum Dynamics and Laser Control of Br_2 in Solid Argon[†]

A. Accardi,[§] A. Borowski,[§] and O. Kühn*,[‡]

Institut für Chemie und Biochemie, Freie Universität Berlin, Takustrasse 3, D-14195 Berlin, Germany, and Institut für Physik, Universität Rostock, D-18051 Rostock, Germany

Received: January 19, 2009; Revised Manuscript Received: April 30, 2009

A five-dimensional reaction surface-vibronic coupling model is introduced to describe the B- to C-state predissociation dynamics of Br_2 occupying a double substitutional lattice site in a face-centered cubic argon crystal at low temperatures. The quantum dynamics driven by a Franck−Condon vertical excitation is investigated, revealing the role of matrix cage compression for efficient nonadiabatic transitions. Vibrational preexcitation of the Br_2 bond in the electronic ground state can be used to access a different regime of predissociation which does not require substantial matrix compression because the Franck−Condon window shifts into the energetic range of the B−C level crossing. Using optimal control theory, it is shown how vibrational preexcitation can be achieved via a pump−dump-type mechanism involving the repulsive C state.

Introduction

Dihalogens embedded in rare gas matrixes are considered as prototypical condensed-phase systems.[1] Besides simple phenomena like vibrational energy relaxation, a host of intriguing processes has been revealed from the interplay between ultrafast nonlinear spectroscopies and theoretical simulations.[2−5] Electronic excitation of the dihalogen triggers a wave packet dynamics involving many nuclear degrees of freedom (DOF) as well as a number of coupled electronic valence states. The cage effect is perhaps the most dramatic manifestation of the interaction between chromophore and matrix motion, which can also lead to electronic transitions.[6] However, the matrix is coupled to the dihalogen's electronic and nuclear DOF in a more intricate way. For instance, the transfer of energy into the matrix upon collision is rather specific as far as collective vibrational motions of the cage are concerned.[7,8] Further, the response of the cage to the change of the electronic wave function can cause excitation of coherent phonon modes whose dynamics is mostly decoupled from the dihalogen's bond vibration. Respective oscillations lasting several picoseconds have been observed with a frequency corresponding to the zone boundary phonon mode of the host crystal.[8−10] Due to the existence of a manifold of closely lying electronic states into which the system is promoted upon laser excitation, nonadiabatic electronic transitions are dominating the excited-state dynamics. These processes can be rather fast; for example, a time scale of about 0.5 ps for a singlet−triplet transition has been observed for ClF in Ar.[11] Theoretical wave packet simulations for the same system using a one-dimensional model even gave a lower limit of 60 fs for the actual spin−flip.[12] A much shorter 1 fs spin−flip time has been predicted for HF in Ar on the basis of nonadiabatic trajectory simulations.[13] Due to the large spin−orbit coupling, the heavier dihalogens like Br_2 or I_2 are usually classified according to Hund's case *c*. Here, the most studied transition is the predissociation between the 0_u^+ and the doubly degenerate 1_u state (usually called B and C states).[14] In the gas phase, the B state has an attractive well while the C state is repulsive. As a consequence of the $\Delta\Omega = 0$ selection rule, the predissociation yield is extremely low.[15] However, in the rare gas environment, the predissociation yield is enhanced considerably, as shown by pressure-dependent studies in the gas to liquid transition region for I_2 in various rare gases.[16]

Recent time-resolved spectroscopic studies by the groups of Apkarian[17] and Schwentner have demonstrated that these systems are unique in providing access to various quantum effects in the condensed phase. For instance, for Br_2 in an Ar wave packet dephasing and rephasing with associated revivals have not only been observed but also manipulated using chirped pulse excitation.[18] This gave access to the vibrational dephasing time in the B state, which was estimated to be as long as 3 ps. At the same time, the electronic dephasing time between the ground X state and the B state has been determined to be longer than 300 fs. For Cl_2 in Ar, it has been shown that the effective chromophore−matrix interaction can be tuned by means of phase-locked pulse pairs. Here, a frequency comb is generated such as to excite wave packets composed of either zero-phonon lines or phonon side bands.[19]

These experimental efforts to control the wave packet dynamics of matrix-isolated dihalogens by means of shaped laser pulses have been accompanied by theoretical simulations, in particular, by Manz and co-workers. For instance, by employing the interference of B- and C-state wave packets, it was shown that for ClF[20] and Cl_2[21] in Ar, the spin state of the wave packet can be controlled on ultrafast time scales. The mechanism builds on the initial preparation of a vibrational superposition state with respect to the bond distance coordinate in the electronic ground state. Different approaches for generating this type of superposition state for homonuclear diatomics have been discussed in refs 21 and 22.

The simulation of coherent laser control necessitates a quantum dynamical approach, although there has been some progress using a semiclassical initial value representation method.[23] In contrast to the surface hopping trajectory method commonly used for these systems,[6,24−29] this requires restriction of the model to a subset of relevant electronic states and nuclear DOF. The quantum control simulations mentioned above have been performed for a three-state model including one coordinate.

[†] Part of the "Robert Benny Gerber Festschrift".

* To whom correspondence should be addressed. E-mail: oliver.kuehn@uni-rostock.de.

[§] Freie Universität Berlin.

[‡] Universität Rostock.

10.1021/jp900551n CCC: $40.75

A different simulation of the cage exit dynamics of F_2 in Ar had been performed for a model including a collective cage coordinate next to the bond distance.[30] Previously, we have introduced a systematic approach to generate multidimensional multistate potential energy surfaces (PES) by combining concepts from reaction surface and vibronic coupling theory.[31] Large-amplitude coordinates are chosen such as to linearly interpolate between relevant points on the PES for different electronic states. For the case of the X- to B-state excitation of Br_2 in Ar, for instance, the two anchor points have been the configurations of the X- and B-state minima. These coordinates are supplemented by harmonic tuning and coupling modes which interact with the electronic states and transitions, respectively.[32] Specifically, ref 31 considered those modes which are important for the B to C transition. The calculation of these PES and state couplings is facilitated by the diatomics-in-molecules (DIM) method as outlined in ref 14 for the case of Br_2 in Ar. Restricting ourselves to certain configurations and states and ordering the harmonic modes according to the strength of their coupling enables one to generate model Hamiltonians with problem-adapted dimensionality.

The quantum dynamics of the reaction surface-vibronic coupling (RSVC) Hamiltonian is conveniently treated using the multiconfiguration time-dependent Hartree (MCTDH) approach.[33,34] It provides a numerically correct solution in between time-dependent Hartree[35] and exact limits. MCTDH has proven to be a versatile tool for multidimensional quantum dynamics[36] including the effects of external laser fields.[37] In ref 38, we have combined a four-dimensional (4D) RSVC Hamiltonian and a MCTDH propagation to study the role of the matrix cage in the B−C predissociation dynamics. It was found that for vertical Franck−Condon excitation, efficient predissociation requires cage compression around the belt of the Br_2 bonding coordinate. Preexcitation of the Br_2 coordinate to the $v = 1$ level was observed to reduce the predissociation yield since the wave packet in the B state samples less of the regions of large matrix deformation.

In the present contribution, we will continue on the topic of B−C predissociation from the perspective of optimal laser control. Controlling the dynamics of molecular systems with tailored laser fields has become a mature subject in recent years (see, e.g., the applications collected in ref 39). However, simulations for high-dimensional systems are scarce due to the numerical overhead necessary to determine optimized laser fields, for example, using the method of optimal control theory (OCT) (see, e.g., ref 40). Therefore, the combination of OCT and MCTDH appears to be a natural choice, and related efforts have been reported.[41,42] Here, we will use the Heidelberg MCTDH package[43] and the OCT implementation of Brown and co-workers.[42]

The paper is organized as follows. Section 2 presents the RSVC Hamiltonian, which is an extension of ref 38 to include the most strongly coupled tuning mode giving a five-dimensional (5D) model. Section 3 starts with an investigation of the laser-driven wave packet dynamics after Franck−Condon excitation, and a comparison is given between the predissociation dynamics of the 4D and 5D models. In a next step, the dependence of the predissociation yield on the vibrational preexcitation of the Br_2 coordinate in the electronic ground state is studied. Subsequently, OCT is used to prepare a preexcited state which shows enhanced predissociation yield as compared with that of the vibrational ground state. The paper is summarized in section 4.

Theory Section

The RSVC Hamiltonian adapted to the description of the four electronic states X, B, and C (doubly degenerate, denoted as C, C′) has been derived in ref 31. It is based on the two mass-weighted large-amplitude coordinates which describe the Br_2 bond elongation (ζ_R) and the deformation of the Ar cage upon changing from the ground- to the B-state minimum configuration (ζ_{X-B}); see Figure 1c and d. Panel b of Figure 1 shows the X-state PES along these two coordinates with all other DOF being frozen at the minimum configuration. Inspecting the shape of the PES, we notice that upon Br_2 bond elongation, the Ar atoms forming a belt around the chromophore move into the space emptied by the expanding Br_2. At the same time, the eight Ar atoms forming two windows through which the Br atoms can pass are pushed outward. In Figure 1a, we show the quasi-adiabatic PES obtained by following the lowest energy along the B and C states. Notice that both large-amplitude coordinates preserve the D_{2h} symmetry of the cage, that is, they are of A_g symmetry. Therefore, they form a crossing seam along the intersection of the B and C states, as indicated by the solid line. This seam runs almost parallel to the ζ_{X-B} axis; the energetic minimum is marked by a filled circle in Figure 1a.

In the spirit of vibronic coupling theory, these large-amplitude coordinates are supplemented by harmonic modes $\{q_i\}$ to give the following Hamiltonian matrix in diabatic representation[31] (note that the DIM Hamiltonian yields complex matrix elements)

$$\mathbf{H} = \begin{pmatrix} T + V_X & 0 & 0 & 0 \\ 0 & T + V_B & -V_{BC}^* & V_{BC'} \\ 0 & -V_{BC} & T + V_C & 0 \\ 0 & V_{BC'}^* & 0 & T + V_{C'} \end{pmatrix} \tag{1}$$

The normal modes are obtained by diagonalizing the Hessian matrix at the electronic ground-state minimum with the two large-amplitude displacements being projected out. They are taken to be dimensionless. Hence, the kinetic energy is defined as

$$T = -\frac{\hbar^2}{2}\left(\frac{\partial^2}{\partial \zeta_R^2} + \frac{\partial^2}{\partial \zeta_{X-B}^2}\right) - \frac{\hbar}{2}\sum_i \omega_i \frac{\partial^2}{\partial q_i^2} \tag{2}$$

The diagonal and off-diagonal elements of the potential energy operator are given by (a,b = X,B,C,C′)

$$V_a = U_a(\zeta_R, \zeta_{X-B}) + \frac{\hbar}{2}\sum_i \omega_i q_i^2 + \sum_i F_{a,i}(\zeta_X, \zeta_{X-B}) q_i \tag{3}$$

and

$$V_{ab} = \sum_i F_{ab,i}(\zeta_X, \zeta_{X-B}) q_i \tag{4}$$

In eq 3, U_a denotes the PES for the large-amplitude coordinates (see Figure 1a,b), the second term is the energy of the oscillators, and the last term the intrastate coupling of the tuning modes taken in linear approximation ($F_{a,i}$ is the gradient along the ith mode). Equation 4 gives the interstate interaction mediated by the coupling modes also taken in linear approximation with gradients $F_{ab,i}$.

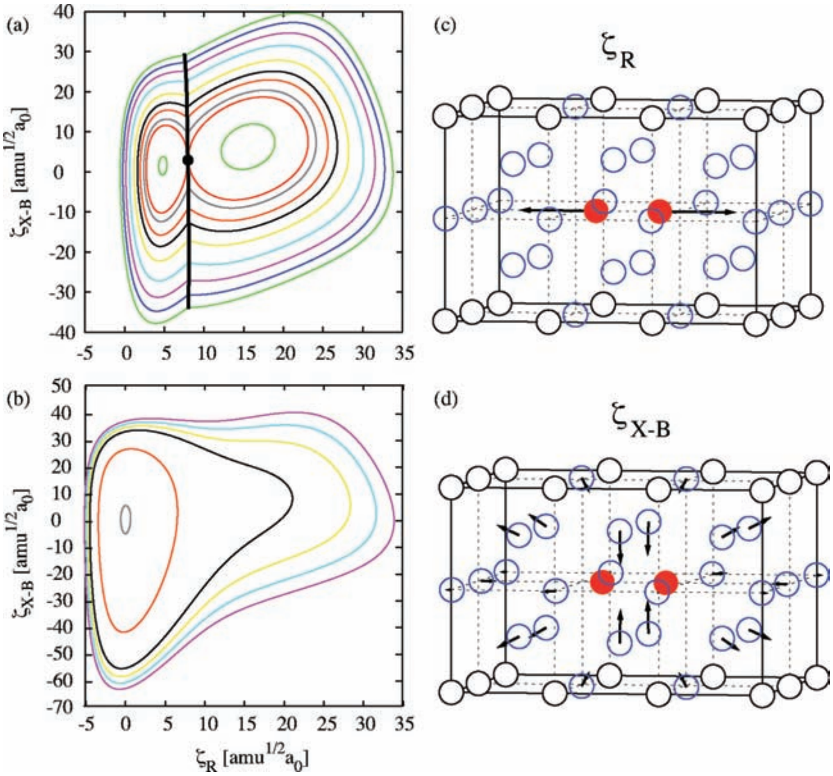

Figure 1. PES along the two large-amplitude coordinates for the (X) ground (panel (b), contour lines at 0.001, 0.035, 0.069, 0.080, 0.090, and 0.100 E_h) and quasi-diabatic (B−C) first excited state (panel a, contour lines at 0.069, 0.072, 0.073, 0.075, 0.077, 0.080,0.085, 0.090, 0.095, and 0.100 E_h). In panel (a), the crossing seam is included as a black line. The minimum along this seam is at $\zeta_R \approx 8$ and $\zeta_{X-B} \approx 3$ amu$^{1/2}a_0$ (dot). Panels (c) and (d) show the mass-weighted atomic displacement vectors for the two large-amplitude coordinates.

The gradients can be used to identify important modes. In ref 31, we have considered coupling modes only. The most strongly coupled modes which are included in the model are shown in Figure 2a,b and denoted as q_1 ($\hbar\omega_1 = 60$ cm^{-1}, B_{3g}) and q_2 ($\hbar\omega_2 = 63$ cm^{-1}, B_{2g}). Displacements with respect to these modes will lead to conical intersections. It turns out that along the crossing seam, the gradient can be approximated to depend on ζ_{X-B} only. The forces on the tuning modes on the B state and for the ground-state minimum configuration are shown in Figure 2d. Apparently, the A_g mode at 61 cm^{-1} sticks out of the otherwise mostly continuous distribution of forces. This mode has been chosen to be included into the model as mode q_3. Motion along this mode corresponds to breathing of the belt Ar atoms; see Figure 2c. The dependence of the gradient on the large-amplitude coordinates has been treated in linear approximation with respect to both ζ_R and ζ_{X-B} and the ground-state minimum configuration

$$F_a(\zeta_R, \zeta_{X-B}) = F_a(\zeta_R = 0, \zeta_{X-B} = 0) + \frac{\partial F_a}{\partial \zeta_R}\zeta_R + \frac{\partial F_a}{\partial \zeta_{X-B}}\zeta_{X-B} \qquad (5)$$

with $F_B = -4.101$, $F_C = -25.96$ (in $10^{-5}E_h$), $\partial F_B/\partial\zeta_R = -2.325$, $\partial F_B/\partial\zeta_{X-B} = 3.828$, $\partial F_C/\partial\zeta_R = -2.025$, and $\partial F_C/\partial\zeta_{X-B} = 3.603$ (in $10^{-5}E_h/a_0$ (amu)$^{-1/2}$).

The interaction with the laser field is described by the Hamiltonian

$$H_{\mathrm{field}}(t) = -\mu\mathcal{E}(t) \qquad (6)$$

where the dipole operator allows for transitions between the X state and the B and C states. It is taken in linear approximation with respect to ζ_R[38] and has been adapted from ref 44. That is, for the transition matrix elements, we use

$$\mu_{Xa} = \mu_{Xa}^{(0)} + \frac{\partial \mu_{Xa}}{\partial \zeta_R}\zeta_R \qquad (7)$$

with $\mu_{XC}^{(0)} = 0.1953ea_0$, $\partial\mu_{XC}/\partial\zeta_R = -0.01047e$ (amu)$^{-1/2}$, $\mu_{XB}^{(0)} = 0.15ea_0$, and $\partial\mu_{XB}/\partial\zeta_R = 0.01e$ (amu.)$^{-1/2}$. For the analytical fields, we assume the form

$$\mathcal{E}(t) = E_0 \exp(-t^2/2\sigma^2)\cos(\omega t) \qquad (8)$$

with amplitude E_0, carrier frequency ω, and width σ.

In the OCT calculations, the following functional is maximized at the final time T[45]

$$J(\mathcal{E}, T) = \langle\Psi(T)|\hat{O}|\Psi(T)\rangle - \alpha\int_0^T \mathrm{d}t \frac{\mathcal{E}^2(t)}{\sin^2(\pi t/T)} \qquad (9)$$

where $\hat{O}$ is the target operator and α the penalty factor.

The four-state 5D time-dependent Schrödinger equation for the wave function $\Psi(t)$ has been solved using the MCTDH method.[43] All coordinates are expressed in terms of a harmonic oscillator discrete variable representation and using the multiset formulation;[33] for details, see Table 1. For the cases of the analytical fields, the equations of motion were integrated in the CMF scheme using the complex Lanczos−Arnoldi and Bulirsch−Stoer methods of orders 15 and 9 for the A vector

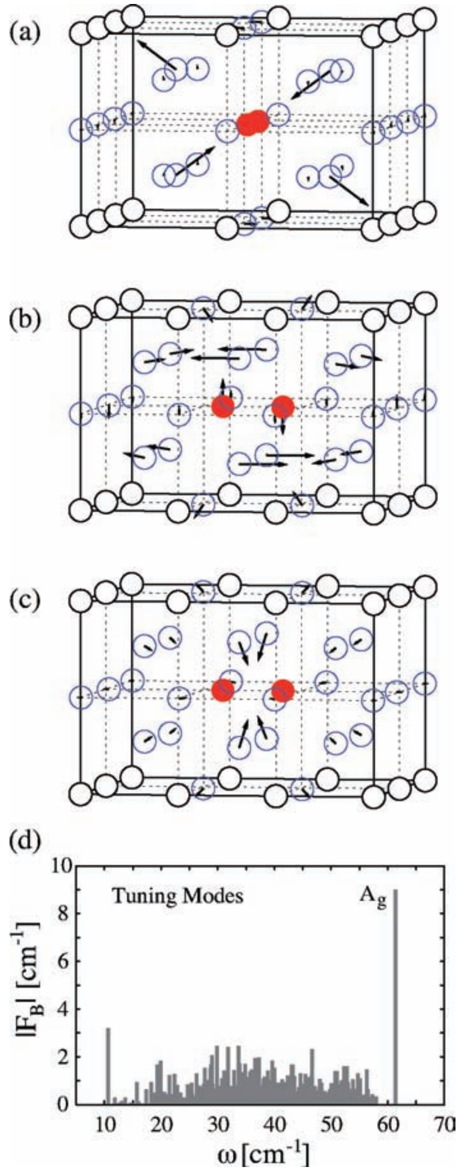

Figure 2. Mass-weighted atomic displacement vectors for the vibronic coupling modes q_1 (B_{3g}) (a) and q_2 (B_{2g}) (b) and the tuning mode q_3 (A_g) (c). (d) The coupling of the ground-state normal modes to the X to B transition upon vertical excitation.

TABLE 1: Parameters Used for the MCTDH Propagation[a]

mode	N_k	X	B	C	C′
ζ_R	160	12	12	12	12
ζ_{X-B}	400	12	12	12	12
q_1	10	4	4	4	4
q_2	10	4	4	4	4
q_3	65	12	12	12	12

[a] All coordinates were expressed in a harmonic oscillator discrete variable representation using N_k grid points; the numbers of SPFs per DOF for the multiset formulation are given in the last columns for the respective electronic states.

and the single-particle functions, respectively. In the OCT propagation, the VMF scheme has been used in combination with an eighth-order Bulirsch−Stoer integrator. The maximum of the lowest natural orbital population has been well below 10^{-10}. A convergence study is provided as Supporting Information.

The predissociation yield will be quantified by the relative population transfer, which is defined as

$$P(t) = \frac{P_C(t) + P_{C'}(t)}{1 - P_X(t)} \tag{10}$$

where $P_a(t)$ is the population of the diabatic state a = X,C,C′.

Results and Discussion

Franck−Condon Excitation. Figure 3a−c shows selected one-dimensional reduced densities for laser excitation from the vibrational ground state in the electronic X state to the B state by a Gaussian pulse, eq 8, having a width of 18 fs, $\omega = 0.09E_h/\hbar$, and $E_0 = 0.005E_h/ea_0$. Under these conditions, about 8% of the population is promoted to the B state. The population transfer to the C state is shown in Figure 3d. Similar to the 4D case studied in ref 38, we observe a stepwise behavior. It finds an explanation in the reduced densities on the B-state PES along the large-amplitude coordinates ζ_R and ζ_{X-B} in Figure 3a and b. It should be noted that appreciable transfer occurs whenever the wave packet passes the crossing seam and is displaced along ζ_{X-B} at the same time. The associated cage compression is required to bring B and C states into resonance. At the same time, the interaction strength of the coupling modes increases; compare Figure 2 of ref 38.

As compared to the previous 4D model, taking into account the tuning mode q_3 clearly influences the wave packet dynamics along the other coordinates. In the given interval up to 2 ps, we observe an energy flow out of the Br_2 bond coordinate (not seen in the 4D calculation).[38] For the collective matrix coordinate ζ_{X-B}, one can distinguish two cases. If ζ_{X-B} and q_3 are out of phase ($t = 750$ and 1700 fs), the ζ_{X-B} motion is decelerated by the tuning mode, which is also reflected in the expectation value of the kinetic energy. For in-phase motion, the matrix coordinate is accelerated and reaches its maximum kinetic energy in the time interval between 1300 and 1400 fs. Comparing the instantaneous energy gap between B and C states, one finds that only at around 1800 fs does this gap become small due to the presence of the q_3 mode. This causes a larger population transfer as seen in Figure 3d (for details, see Supporting Information and ref 46).

Vibrational Preexcitation-Dependent Dynamics. Franck−Condon excitation from the vibrational ground state generates a B-state wave packet which is energetically about $0.016E_h$ above the crossing seam upon first passage. As a consequence, efficient B to C transfer requires a deformation of the matrix cage, as shown in the previous section. Another means for establishing resonance would be an excitation deeper into the B-state PES. By virtue of the Franck−Condon factors, this is possible for vibrationally excited initial states only. Such states have been used previously, for example, for coherent spin control[20] or for modifying the cage exit dynamics for HCl in solid Kr.[47] Here, we have studied the predissociation yield for different initial vibrational states in the electronic ground state for $v = 0-10$. For simplicity, these initial states have been obtained as vibrational eigenstates of one-dimensional PES cuts along the Br_2 coordinate ζ_R with all other DOF frozen at the minimum. The frequency of the laser field has been adjusted such as to be in resonance with the X to B transition, transferring about 8% of the X-state population to the B state for the cases considered.

The population dynamics for four different initial conditions is compared in Figure 4. First, the predissociation yield decreases with v until $v = 5$ but then increases to reach a maximum at $v = 8$, after which it decreases again. The case of $v = 1$ has already been discussed within the 4D model in ref 38. There,

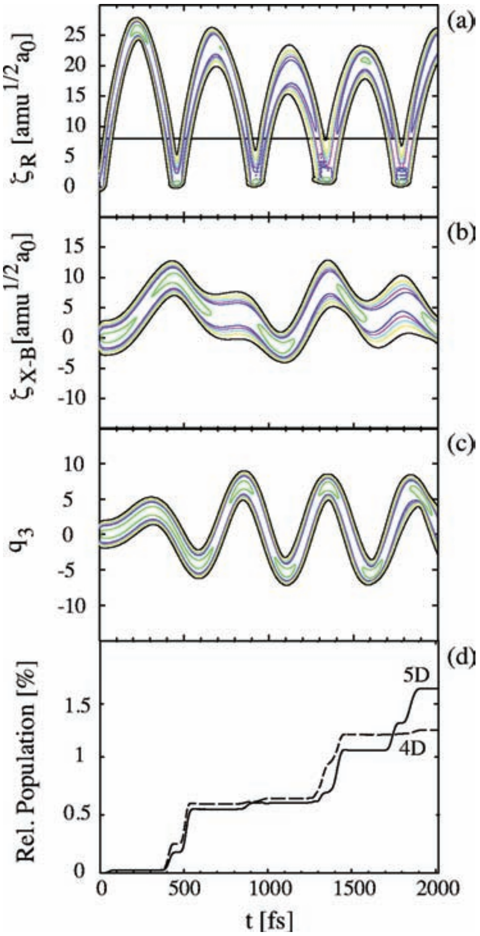

Figure 3. Time-dependent reduced B-state densities for (a) the Bromine coordinate $\rho^{(B)}(\zeta_R,t)$ (isodensity values of 0.001, 0.003, 0.005, 0.007, 0.01, and 0.03), (b) the matrix coordinate $\rho^{(B)}(\zeta_{X-B},t)$ (isodensity values of 0.002, 0.004, 0.006, 0.008, 0.01, and 0.02), and (c) the tuning mode $\rho^{(B)}(q_3,t)$ (isodensity values of 0.001, 0.003, 0.005, 0.007, 0.01, and 0.03). Panel (d) compares the relative C-state population, eq 10, of the present 5D to that of the former 4D model,[38] which did not include the tuning mode.

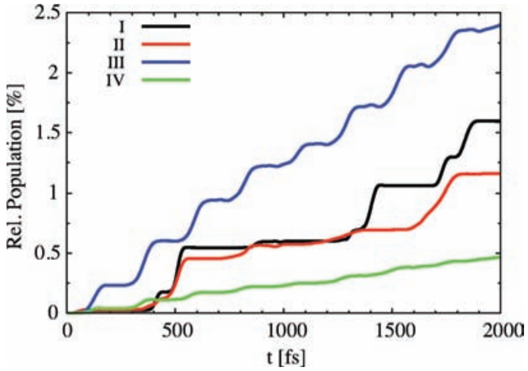

Figure 4. Population dynamics (relative C-state population, eq 10) for excitation from different vibrational states in the electronic ground state, (I) $v = 0$, (II) $v = 1$, (III) $v = 8$, and (IV) $v = 10$. The pulse parameter of the Gaussian pulse have been set to $\sigma = 18$ fs, and $E_0 = 0.005E_h/ea_0$. The following frequencies have been found to give maximum population transfer: $\omega_0 = 0.092$, 0.0825, 0.0606, and $0.0567E_h/\hbar$.

the reasons for the decrease of the predissociation yield had been identified. For excitation deeper into the B-state PES, the wave packet samples less of the anharmonicity, reducing the excitation of the matrix DOF and thus the B−C coupling strength. At the same time, the kinetic energy upon passing the crossing seam configuration is still too high to compensate for the reduced coupling by having a better resonance. In passing, we note that this behavior can also be rationalized in terms of Landau−Zener theory, which gives the nonadiabatic transfer rate proportional to the ratio of the squared coupling matrix element and the velocity at the crossing point.[1] Starting with $v = 5$, this situation changes, and for $v = 8$, one has the case where the energy of the wave packet is approximately in resonance with the crossing seam. The crossing seam has an energy of $0.074E_h$, which corresponds to the fourth vibrational level in the uncoupled B state. The energy of the $v = 8$ level in the X state is $0.0133E_h$, which, together with the excitation energy of $0.0606E_h$, matches approximately the energy of the crossing seam along the ζ_R coordinate. Therefore, the steplike increase of the predissociation yield in Figure 4 results from the small-amplitude vibration of the Br$_2$ coordinate in the B state. Each time the wave packet hits the curve crossing (or the barrier in the quasi-adiabatic picture), part of it is transferred to the C state. Moving even deeper into the potential well for higher vibrational preexcitation, transfer becomes possible only by means of potential tunneling through the predissociation barrier. Due to the heavy mass of Br$_2$, the predissociation yield drops dramatically.

OCT Preparation of a Vibrationally Excited Ground State. Vibrational preexcitation of matrix-isolated heterodimers has been demonstrated, for example, for HCl in Kr in[47] by direct IR excitation. This, however, is not possible for homodimers like Br$_2$, and excitation strategies involving excited electronic states have to be used in analogy to Tannor's pump−dump scheme.[48] In fact, this stimulated Raman type of excitation has been demonstrated for gas-phase K$_2$, where ground-state wave packets could be generated with mean quantum numbers ranging from 4 to 18 depending on the laser pulse parameters (wavelength, pulse delay).[49] In the strong field regime, nonequilibrium ground-state distributions can be generated by a vibrational hole-burning mechanism.[50,51] In contrast, in refs 21 and 22, the goal has been to selectively excite a single vibrational state in the electronic ground state and at the same time leave no population in the electronic excited state. This was achieved by means of narrow bandwidth lasers with durations of tens of picoseconds, which are state-selective within an effective one-dimensional model of Cl$_2$ in Ar.

In the following, we will show that OCT can answer the question of preparing vibrationally preexcited levels in the electronic ground state of Br$_2$. To this end, the goal in eq 9 has been set to populate the $v = 8$ state discussed above, that is, $\hat{O} = |v = 8\rangle\langle v = 8|$. Eventually, this state will be used as an initial state for investigation of the B−C predissociation. In order to avoid having a wave packet moving on the B state from the OCT pulse already, we have chosen to focus on a mechanism which involves the C-state PES. Note that this choice is, of course, dictated by the already-developed model Hamiltonian. Any other excited state would be equally well-suited for the present purpose. The time interval considered below (550 fs) exceeds the timespan of ∼300 fs required by the C-state wave packet to return to the Franck−Condon region. In order to keep the model simple, we have chosen to neglect the C-state wave packet for the simulations reported in the following subsection.

In the Franck−Condon region, the C-state PES is repulsive, and the wave packet moves rapidly out of the region where it overlaps with the $v = 8$ state. This suggests a reasonable final time of $T = 50$ fs in eq 9. The initial guess field has been chosen as $\mathcal{E}(t) = E_0 \sin^2(\pi t/T) \cos(\omega_0(t - T/2))$, with $E_0 = 0.005E_h/ea_0$ and $\omega_0 = 0.1099E_h/\hbar$ (vertical transition at the minimum).

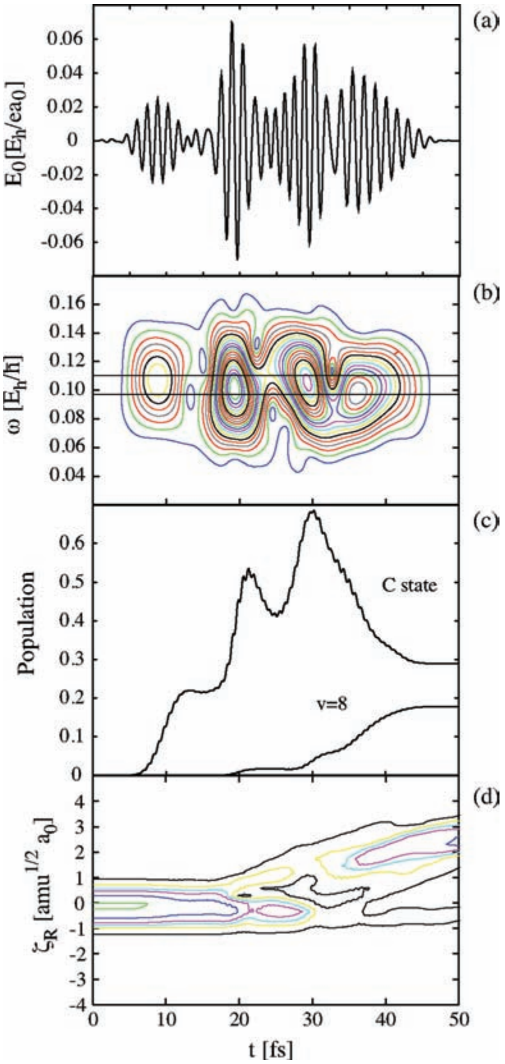

Figure 5. (a) OCT pulse after 200 iterations (see text). (b) XFROG trace of the OCT pulse (contours from 0.2 to 4 in steps of 0.2). The gate function in eq 11 has been a rectangle of width $41\hbar/E_h$ with Gaussian tails of the same width; see ref 42. The two horizontal lines are drawn to indicate the vertical transitions from the $v = 0$ and 8 vibrational states in the X state to the C state. (c) Population of the C state and of the target state $v = 8$ in the electronic ground state. (d) Time-dependent reduced 1D X-state density for the bromine coordinate $\rho^{(B)}(\zeta_R,t)$ (isodensity values of 0.05, 0.15, 0.25, 0.35, 0.55, and 0.85) during the OCT pulse.

In order to obtain a J functional different from 0, it was necessary to use a very small penalty factor of 0.000025 au for the first iteration, which is increased to 0.08 au for the second iteration; subsequently, it is kept constant at a value of 0.1 au. Note that the field does not change appreciably during this procedure, except for its amplitude (see Supporting Information).

After 200 iterations, the iterative change in J becomes rather small, and about 17% of the total population is transferred into the target, another one-third of the population remains on the C state (see Figure 5c), and the rest is distributed over the lowest vibrational levels with $v \neq 8$. In other words, OCT generates a vibrational wave packet in the X state, whose reduced density along ζ_R is shown in Figure 5d.

The population change of the target state in Figure 5c proceeds in three steps. The optimized pulse in Figure 5a consists of four subpulses, whose action can be rationalized from the XFROG trace (see ref 42)

$$I_{\mathrm{XFROG}}(\omega,\tau) = \left|\int \mathrm{d}t\,\mathcal{E}(t)G(t-\tau)\mathrm{e}^{-\mathrm{i}\omega t}\right|^2 \qquad (11)$$

in panel (b) of Figure 5. Here, $G(t)$ is a rectangular gate function with Gaussian tails as in ref 42. The first subpulse is resonant to the vertical X to C transition starting from the vibrational ground state ($0.1099E_h$; upper horizontal line in Figure 5b). It populates the C state by about 20%, but there is no population of the target state. The second subpulse has a negative chirp; it excites the C state and stimulates population down to the X state at the same time. The chirp brings the center frequency down to accommodate the transition energy from the C to the $v = 8$ state ($0.0966E_h$; lower horizontal line). The action of the third subpulse is rather similar to that of the second one. Finally, a fourth subpulse being resonant to the transition from the C to the $v = 8$ state captures part of the propagating C-state wave packet and pumps it down to the X state.

One should notice that the peak intensity of the OCT field is on the order of 10^{14} W cm^{-2}, that is, about 2 orders of magnitude larger than the estimated damage threshold for Br_2 in solid Ar (N. Schwenter, private communication). Preliminary calculations using the final field from the present optimization and gradually increasing the penalty to 0.2 gave a reduction of the field intensity by a factor of 4, of course, at the expense of the control yield. However, the pump−dump-like scheme is not appreciably modified, that is, the mechanistic aspects of the proposed control pathway do carry to the regime of lower intensities.

Predissociation Starting From the OCT Ground-State Wave Packet. The time evolution of the ground-state wave packet after the OCT pulse is shown in Figure 6a. It obeys a rather regular behavior, which suggests a simple scheme for excitation to the B state. For instance, a short pulse could promote this wave packet to the B state whenever it is at its outer turning point. This has the advantage that the wave packet is rather compact. Compared to the $v = 8$ initial state, however, the vertical transition from the outer turning point is a bit below the B−C level crossing. Given the energetic spread of wave packet and the pulse spectrum, this should not lead to a substantial difference in the predissociation mechanism.

For the purpose of illustration, we have performed a propagation with a Gaussian field of width $\sigma = 18$ fs, frequency $\omega = 0.0606E_h/\hbar$ (resonant transition which gives maximum population transfer from the $v = 8$ state), and strength $E_0 = 0.005E_h/ea_0$, which is centered at 185 fs; see Figure 6b. To simplify matters, we have set the C-state population from the OCT run equal to 0 and renormalized the ground-state wave packet. The resulting predissociation dynamics is shown in Figure 6c. The population of the B state again amounts to about 8%. Compared to the case of excitation from the $v = 8$ eigenstate, the dynamics looks rather similar, that is, one observes steps whenever the wave packet hits the barrier region. Two points should be emphasized. First, it is surprising that the predissociation yield after 550 fs is almost the same. After all, one compares excitation from rather different initial states, and we have not even attempted to optimize the pulse parameters. Second, one could, in principle, envisage a simple extension of this control scheme, which consists of a train of pulses acting each time the wave packet is located at its outer turning point.

Summary

The nonadiabatic laser-driven quantum dynamics of a dihalogen in a rare gas matrix has been described on the basis of MCTDH wave packet propagations for a model DIM Hamiltonian. The latter combined large-amplitude reaction surfaces

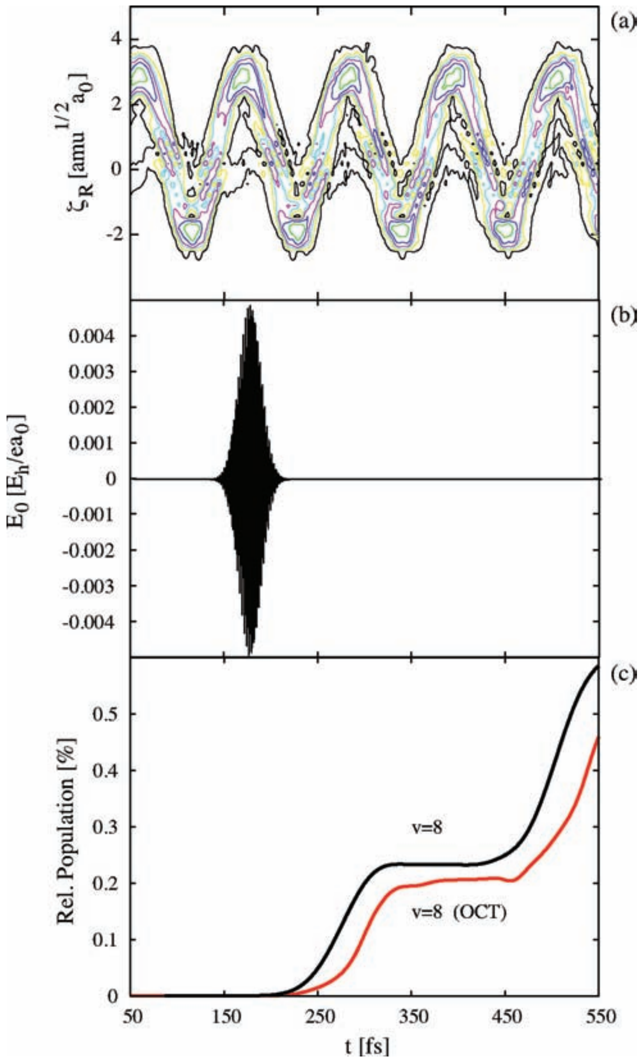

Figure 6. (a) Time-dependent reduced X-state density for the bromine coordinate $\rho^{(B)}(\zeta_R,t)$ (isodensity values of 0.05, 0.15, 0.25, 0.35, 0.55, and 0.85) after the OCT pulse is over. (b) Gaussian pulse ($\sigma = 18$ fs, $E_0 = 0.005E_h/ea_0$, $\omega = 0.0606E_h/\hbar$) promoting part of the ground-state wave packet to the B state. (c) Population dynamics (relative C-state population, eq 10) for $v = 8$ and the OCT wave packet (at 50 fs) as the initial state.

with vibronically coupled normal modes. Although restricted to five DOF, the extension to higher dimensions, in principle, is straightforward since the PES and couplings can easily be generated in the DIM approach. Concerning the specific case considered here, the rather dense spectrum of coupled tuning modes, for instance, leaves open the question of how to choose a reasonable model below the full-dimensional one (whose dimensionality is determined by the number of atoms in the simulation box). In principle, to handle the full-dimensional situation, density matrix theory could be appropriate,[1] although MCTDH in the multilayer formulation might even allow for a numerically exact wave packet propagation.[52] On the other hand, the modest effort for calculating DIM PES and their couplings should be well-suited for the application of trajectory-based MCTDH.[53]

The RSVC-MCTDH approach has been applied to study the laser control of the B- to C-state predissociation dynamics. First, it was observed that the predissociation yield strongly depends on that vibrational level which is initially populated in the electronic ground state. There is a maximum reached for $v = 8$ which corresponds to the situation where the wave packet is launched in the range of the B−C curve crossing. The predissociation probability for the B to C crossing has been experimentally estimated from the broadening of zero-phonon lines to be 5% per vibrational round trip.[54] This is considerably more than that observed in the present simulation. A possible source of error could be the Br−Ar interaction potential, which has been extracted from photoelectron spectroscopy (for details, see ref 14).

Second, using OCT, it was shown that a ground-state wave packet with dominating $v = 8$ character can be prepared by a multiple pump−dump-like mechanism involving the C state. Part of this ground-state wave packet can subsequently be excited by a simple Gaussian-shaped pulse to give approximately the same predissociation yield as the idealized case of a stationary initial state.

Acknowledgment. This work has been financially supported by the Deutsche Forschungsgemeinschaft (Sfb 450).

Supporting Information Available: Additional results and parameters. This material is available free of charge via the Internet at http://pubs.acs.org.

References and Notes

(1) May, V.; Kühn, O. *Charge and Energy Transfer Dynamics in Molecular Systems*, 2nd revised and enlarged edition; Wiley-VCH: Weinheim, Germany, 2004.

(2) Jungwirth, P.; Gerber, R. B. *Chem. Rev.* **1999**, *99*, 1583.

(3) Apkarian, V.; Schwentner, N. *Chem. Rev.* **1999**, *99*, 1481.

(4) Bargheer, M.; Borowski, A.; Cohen, A.; Fushitani, M.; Gerber, R.; Gühr, M.; Hamm, P.; Ibrahim, H.; Kiljunen, T.; Korolkov, M.; Kühn, O.; Manz, J.; Schmidt, B.; Schröder, M.; Schwentner, N. Coherence and Control of Molecular Dynamics in Rare Gas Matrices. In *Analysis and Control of Ultrafast Photoinduced Reactions*; Kühn, O., Wöste, L., Eds.; Springer Verlag: Heidelberg, Germany, 2007; Vol. 87, p 257.

(5) Gühr, M.; Bargheer, M.; Fushitani, M.; Kiljunen, T.; Schwentner, N. *Phys. Chem. Chem. Phys.* **2007**, *9*, 779.

(6) Niv, M.; Bargheer, M.; Gerber, R. B. *J. Chem. Phys.* **2000**, *113*, 6660.

(7) Eshet, H.; Ratner, M.; Gerber, R. *Chem. Phys. Lett.* **2006**, *431*, 199.

(8) Fushitani, M.; Schwentner, N.; Schröder, M.; Kühn, O. *J. Chem. Phys.* **2006**, *124*, 024505.

(9) Gühr, M.; Bargheer, M.; Schwentner, N. *Phys. Rev. Lett.* **2003**, *91*, 085504.

(10) Gühr, M.; Schwentner, N. *Phys. Chem. Chem. Phys.* **2005**, *7*, 760.

(11) Bargheer, M.; Niv, M. Y.; Gerber, R. B.; Schwentner, N. *Phys. Rev. Lett.* **2002**, *89*, 108301.

(12) Bargheer, M.; Gerber, R. B.; Korolkov, M. V.; Kühn, O.; Manz, J.; Schröder, M.; Schwentner, N. *Phys. Chem. Chem. Phys.* **2002**, *4*, 5554.

(13) Cohen, A.; Gerber, R. B. *Chem. Phys. Lett.* **2007**, *441*, 48.

(14) Borowski, A.; Kühn, O. *Theor. Chem. Acc.* **2007**, *117*, 521.

(15) Heaven, M. C. *Chem. Soc. Rev.* **1986**, *15*, 405.

(16) Lienau, C.; Zewail, A. H. *Chem. Phys. Lett.* **1994**, *222*, 224.

(17) Bihary, Z.; Karavitis, M.; Apkarian, V. A. *J. Chem. Phys.* **2004**, *120*, 8144.

(18) Gühr, M.; Ibrahim, H.; Schwentner, N. *Phys. Chem. Chem. Phys.* **2004**, *6*, 5353.

(19) Fushitani, M.; Bargheer, M.; Gühr, M.; Ibrahim, H.; Schwentner, N. *J. Phys. B* **2008**, *41*, 074013.

(20) Korolkov, M. V.; Manz, J. *J. Chem. Phys.* **2004**, *120*, 11522.

(21) Alekseyev, A. B.; Korolkov, M. V.; Kühn, O.; Manz, J.; Schröder, M. *J. Photochem. Photobiol., A* **2006**, *180*, 262.

(22) Korolkov, M. V.; Manz, J. *J. Chem. Phys.* **2007**, *126*, 174306.

(23) Batista, V.; Brumer, P. *J. Phys. Chem. A* **2001**, *105*, 2591.

(24) Coker, D. F. In *Computer Simulation in Chemical Physics*; Allen, M. P., Tildesley, D. J., Eds.; Kluwer Academic: Dordrecht, The Netherlands, 1993; p 315.

(25) Gersonde, I. H.; Gabriel, H. *J. Chem. Phys.* **1993**, *98*, 2094.

(26) Batista, V. S.; Coker, D. F. *J. Chem. Phys.* **1997**, *106*, 6923.

(27) Chaban, G.; Gerber, R. B.; Korolkov, M. V.; Manz, J.; Niv, M. Y.; Schmidt, B. *J. Phys. Chem. A* **2001**, *105*, 2770.

(28) Bargheer, M.; Cohen, A.; Gerber, R.; Gühr, M.; Korolkov, M.; Manz, J.; Niv, M.; Schröder, M.; Schwentner, N. *J. Phys. Chem. A* **2007**, *111*, 9573.

(29) Cohen, A.; Gerber, R. B. *Chem. Phys. Lett.* **2008**, *453*, 173.

(30) Gerber, R. B.; Korolkov, M. V.; Manz, J.; Niv, M. Y.; Schmidt, B. *Chem. Phys. Lett.* **2000**, *327*, 76.

(31) Borowski, A.; Kühn, O. *J. Photochem. Photobiol., A* **2007**, *190*, 169.

(32) *Conical Intersections*; Domcke, W., Yarkony, D. R., Köppel, H., Eds.; World Scientific: River Edge, NJ, 2004.

(33) Beck, M. H.; Jäckle, A.; Worth, G. A.; Meyer, H.-D. *Phys. Rep.* **2000**, *324*, 1.

(34) Meyer, H.; Worth, G. A. *Theor. Chem. Acc.* **2003**, *109*, 251.

(35) Gerber, R. B.; Buch, V.; Ratner, M. A. *J. Chem. Phys.* **1982**, *77*, 3022.

(36) *Multidimensional Quantum Dynamics: MCTDH Theory and Applications*; Meyer, H.-D., Gatti, F., Worth, G., Eds.; VCH-Wiley: Weinheim, Germany, 2009.

(37) Naundorf, H.; Worth, G. A.; Meyer, H.-D.; Kühn, O. *J. Phys. Chem. A* **2002**, *106*, 719.

(38) Borowski, A.; Kühn, O. *Chem. Phys.* **2008**, *347*, 523.

(39) *Analysis and Control of Ultrafast Photoinduced Reactions*; Kühn, O., Wöste, L., Eds.; Springer: Heidelberg, Germany, 2007; Vol. 87.

(40) Rabitz, H. *Theor. Chem. Acc.* **2003**, *109*, 64.

(41) Wang, L.; Meyer, H.-D.; May, V. *J. Chem. Phys.* **2006**, *125*, 014102.

(42) Schröder, M.; Carreon-Macedo, J.-L.; Brown, A. *Phys. Chem. Chem. Phys.* **2008**, *10*, 850.

(43) Worth, G.; Beck, M.; Jäckle, A.; Meyer, H.-D. *The MCTDH Package*, Version 8.3; University of Heidelberg: Heidelberg, Germany, 2002; http://www.pci.uni-heidelberg.de/tc/usr/mctdh/.

(44) Tellinghuisen, J. *J. Chem. Phys.* **2003**, *118*, 1573.

(45) Sundermann, K.; de Vivie-Riedle, R. *J. Chem. Phys.* **2000**, *110*, 1896.

(46) Borowski, A. Ph.D. Thesis. Freie Universität, Berlin, Germany, 2008.

(47) Berghof, V.; Schwentner, N. *J. Chem. Phys.* **2002**, *117*, 8256.

(48) Tannor, D. J.; Kosloff, R.; Rice, S. A. *J. Chem. Phys.* **1986**, *85*, 5805.

(49) Pausch, R.; Heid, M.; Chen, T.; Schwoerer, H.; Kiefer, W. *J. Raman Spectrosc.* **2000**, *31*, 7.

(50) Banin, U.; Bartana, A.; Kosloff, R. *J. Chem. Phys.* **1994**, *101*, 8461.

(51) Kühn, O.; Malzahn, D.; May, V. *Int. J. Quantum Chem.* **1996**, *57*, 343.

(52) Wang, H.; Thoss, M. *J. Chem. Phys.* **2003**, *119*, 1289.

(53) Lasorne, B.; Robb, M. A.; Worth, G. A. *Phys. Chem. Chem. Phys.* **2007**, *9*, 3210.

(54) Ibrahim, H.; Gühr, M.; Schwentner, N. *J. Chem. Phys.* **2008**, *128*, 064504.

JP900551N